Proceedings of the ASME 2014 Pressure Vessels & Piping Conference
PVP2014
July 20-24, 2014, Anaheim, California, USA

PVP2014-28797

REVIEW AND DEVELOPMENT OF PRIMARY LOAD ELEVATED TEMPERATURE DESIGN RULES

David J. Dewees
The Babcock & Wilcox Company
Barberton, Ohio, USA
djdewees@babcock.com

Benjamin F. Hantz IV
Valero Energy Corporation
San Antonio, TX, USA
ben.hantz@valero.com

ABSTRACT

A recent high temperature steam header case study is extended here to include alternate methods of review, including elastic stress and isochronous strain analysis and accompanying limits. The previous creep analysis was formulated to be exactly consistent with the allowable stress basis, such that alternate design analysis methods and criteria could be rigorously compared. In the current work, the selection of the appropriate limits for elastic results is investigated, as discussed in previous literature, which is motivated by stress redistribution characteristics of the primary (and secondary) loading in a typical header. Next, use of isochronous stress-strain curves generated from the same consistent (Omega) creep model are used for analysis and compared to candidate strain limits. The analyses show that both elastic and isochronous analysis have potential for effective creep design in the context of current high temperature design modernization activities. Finally, multiaxial creep behavior and its effect on detailed creep, elastic and isochronous stress-strain analyses and corresponding limits is also introduced.

INTRODUCTION

Experience and rule-based design methods for equipment operating in the creep regime have been used successfully for many decades (for example [1] and [2]). Additionally, Design-by-Analysis (DBA) approaches to design (e.g. ASME Section III, Subsection NH [3]) and analysis (EDF Procedure R5 [4]) have evolved since the 1970's in the nuclear industry. More recent efforts have extended creep (or elevated temperature) DBA by providing a specific material model and accompanying material data for creep-dominated (as opposed to fatigue-dominated or creep-fatigue interaction) operation ([5],[6]). Specifically, the Omega creep model ([7],[8]) standardized in Part 10 of API 579 ([5],[6]) provides a unique relationship between rupture and creep strain vs. time behavior through introduction of a Larson-Miller based parameter termed Omega (Ω). In [9], this unique relationship between the creep curve and the rupture Larson-Miller Parameter (LMP) was found to be very useful in maintaining a direct relationship with allowable stress-based design (e.g. [1] and [2]), and was termed a "consistent" material model. This paper is a direct extension of that work ([9],[10]), where the consistent (Omega) material model was used to investigate the basic sizing of a Grade 91 (9Cr-1Mo-V) superheater header typical of modern fossil utility power plants. This work is motivated by lack of a consensus elevated temperature design method, and the current focus on modernization of historically experience-based design codes such as ASME Section I [1].

A key result from the previous work was that consistent analysis showed a much lower design load for the header (limited by the penetration and ligament regions and not the plain cylinder itself) than would be expected from allowable stress-based design. This could be due simply to an elevated stress existing in this region, since the stress in the ligaments is not directly considered in most experience-based (area replacement) rules. Inconsistencies are possible relative to detailed analysis (and perhaps even experience) which is evidenced by the complete revision of such penetration rules to be based on local stress [11] in the ASME Section VIII Division 2 rewrite [12]. In elevated temperature design, the situation is more complex. For example, the stress redistribution characteristics in vessel junction regions was investigated by Becht [13], and it was found through transient inelastic analysis that pressure-induced discontinuity stresses did not in fact relax to the degree expected. Extension of this work to the case of a typical header is a primary focus of the current work. This makes elastic analysis a natural starting point for the discussion, and is the first focus of this paper.

The second topic investigated is the use of isochronous stress-strain curves with strain allowables, as a design and analysis option of intermediate complexity, and potentially, accuracy (relative to detailed time-dependent inelastic analysis). The isochronous stress strain curves are developed from the same consistent material model used in the detailed

inelastic analysis ([9], [10]). Curves are used corresponding to an assumed design case (100,000 hours) and an operating case (300,000 hours).

In all cases, review and analysis remains restricted to the uniaxial creep curve/property case for simplicity. As discussed at the end of the paper, consideration of multiaxial creep is the next major step in design method review and development.

SUMMARY OF PREVIOUS WORK

The relationship between the uniaxial Omega creep and damage model and the (creep) rupture LMP was presented by Prager in sources such as [8]. The straightforward exploitation of this relationship for assessment of allowable stress based results was presented in [9]. The application of the model was demonstrated first on a simple cylinder and then for a heat recovery steam generator (HRSG) high pressure secondary superheater outlet header (taken from [14]).

The header outer diameter was 14.25 inches (361.95 mm) and the wall thickness was 1.60 inches (40.64 mm) corresponding to the design pressure of 2575 psig (17.754 MPa) and the design temperature of 1085°F (585°C). Two stubs were oriented at 45° to vertical, and each had an outer diameter of 4.50 inches (114.30 mm) and a wall thickness of 0.531 inches (13.487 mm). The reinforcing fillet leg length between the stub and header was taken as equal to the stub thickness. The original finite element model based on these dimensions is shown in Figure 1. Repeating symmetry boundary conditions are used (no header axial displacement at one end of the plain cylinder, and equal axial displacement of the entire other end). Rigid body motion is prevented by specifying zero hoop direction motion at both ends of the plain cylinder.

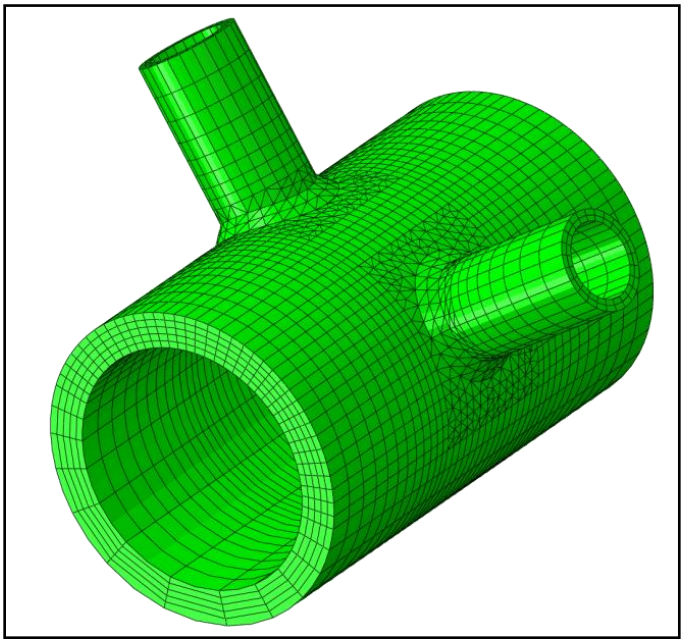

FIG. 1: ORIGINAL SUPERHEATER FINITE ELEMENT MESH (from [14] and [10])

The intended operating conditions were assumed to be 2430 psig (16.754 MPa) and 1050°F (565.6°C) for illustration. As demonstrated in [10], the example header met all Design-by-Rule requirements of [1], including area replacement rules with substantial margin; 2.43 in^2 (1567.7 mm^2) required vs. 5.95 in^2 (3838.7 mm^2) available. The previous elastic stress results are shown in Figure 2. All previous and current analysis is performed with the commercial finite element software Abaqus [15].

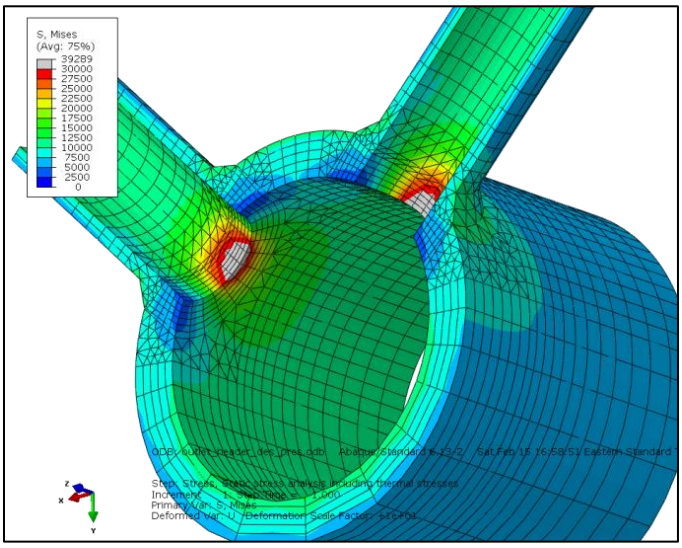

FIG. 2: ORIGINAL ELASTIC FEA DESIGN PRESSURE RESULTS (2575 psig)

Temperature-dependent thermal and elastic material properties for Grade 91 were taken from [16]. Creep properties were developed in [9], and are summarized in Table 1. These properties were used with the (uniaxial) Omega creep strain and damage model, which can be summarized as follows for the secondary and tertiary regions of a standard creep curve [6]:

$$\log \dot{\varepsilon}_0 = -\left(a_0 + \frac{a_1 + a_2 S_l + a_3 S_l^{\,2} + a_4 S_l^{\,3}}{T_{abs}} \right) \tag{1}$$

$$\log \Omega = b_0 + \frac{b_1 + b_2 S_l + b_3 S_l^{\,2} + b_4 S_l^{\,3}}{T_{abs}} \tag{2}$$

$$\dot{\varepsilon}_t = \dot{\varepsilon}_o e^{\Omega \varepsilon_t} = \frac{\dot{\varepsilon}_o}{1 - \int_0^t \Omega \dot{\varepsilon}_o dt} \tag{3}$$

Primary creep was also included using the extended uniaxial Omega model [17] with the following assumptions:

$$\begin{aligned} \dot{\varepsilon}_{op} &\approx 200 \dot{\varepsilon}_o \\ \Omega_p &\approx 20 \Omega \end{aligned} \tag{4}$$

$$\dot{\varepsilon}_p = \dot{\varepsilon}_{op} e^{-\Omega_p \varepsilon_p} = \frac{\dot{\varepsilon}_{op}}{1 + \int_0^t \Omega_p \dot{\varepsilon}_{op} dt} \quad (5)$$

Such that the complete creep strain model is:

$$\dot{\varepsilon}_c = \dot{\varepsilon}_p + \dot{\varepsilon}_t = \dot{\varepsilon}_{op} e^{-\Omega_p \varepsilon_p} + \dot{\varepsilon}_o e^{\Omega \varepsilon_t} \quad (6)$$

TABLE 1
GRADE 91 OMEGA CONSTANTS FROM [9]

	For Units of ksi, degrees R	For Units of MPa, degrees K		For Units of ksi, degrees R	For Units of MPa, degrees K
a_0	-32.36	-32.36	b_0	-2.0	-2.0
a_1	70650.0	38584.0	b_1	7200.0	4698.8
a_2	-2880.0	3188.4	b_2	-1500.0	-833.3
a_3	-5139.5	-2855.3	b_3	0.0	0.0
a_4	0.0	0.0	b_4	0.0	0.0

The primary conclusion of [10] was that detailed inelastic analysis predicted significantly fewer design hours to rupture than the allowable stress itself would suggest. This was based on an analysis formulated to match (in part) the allowable stress definition. That is, with 1.5 times the desired load applied, an analysis must reach 100,000 hours with properties based on average creep rupture to meet the intent of the allowable stress basis. In fact, the stub region limited the analysis and predicted rupture in only roughly 30,000 hours at 1.5 times design load, which is shown in Figure 3.

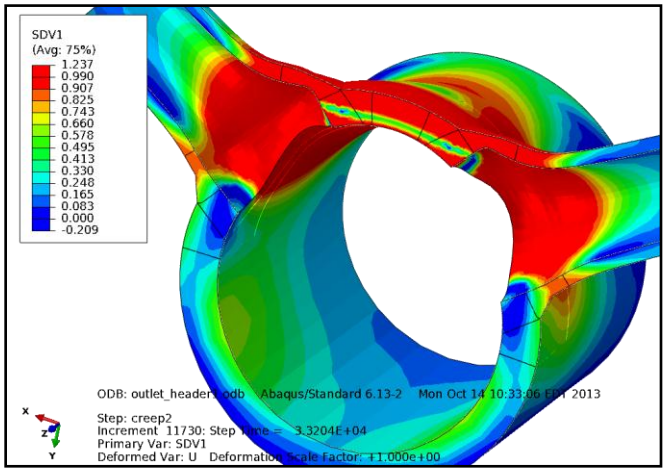

FIG. 3: ORIGINAL INELASTIC FEA 1.5x DESIGN PRESSURE RESULTS (3862 psig, 26.628 MPa, from [9])

In Figure 3 "SDV1" is (uniaxial) creep damage and directly represents the fraction of rupture life consumed. This is not to suggest that the design is necessarily deficient; however, at the least the margin in the design is not uniform. This variation in margin is likely enveloped by the substantial factor embedded in the allowable stress itself (i.e. 1.5 times the design load must give 100,000 hours of predicted operation).

Finally, the previous analysis concluded that simplified elevated temperature limit load procedures led to inconsistent results relative to detailed inelastic analysis and likely require further investigation before incorporation into codes such as [1] and [12].

ELASTIC FINITE ELEMENT ANALYSIS

The previous analysis modeled one full row of header stubs (two stubs in this case) to allow application of multiple external loads and moments (in [14]). The current analysis (and the analysis in [10]) does not consider external loading, such that the model is simplified and refined, as shown in Figure 4 and Figure 5. The updated model consists of exactly one quarter of the previous model (Figure 1), and the new symmetry planes are colored in blue in Figure 4 and Figure 5. As in [10], temperature-dependent material properties from [16] are used for the FEA. The finite element mesh is made up of hexahedral elements; both linear (8 node, full integration) and quadratic (20 node, reduced integration) elements are analyzed to verify mesh convergence. For the structural boundary conditions, appropriate restraints are applied to both ends of the model to simulate the effects of a continuous header (using kinematic constraints). Internal pressure is applied to the inner surfaces and axial pressure thrusts (corrected for symmetry) are applied to the header stub end and the header shell face opposite the restrained end.

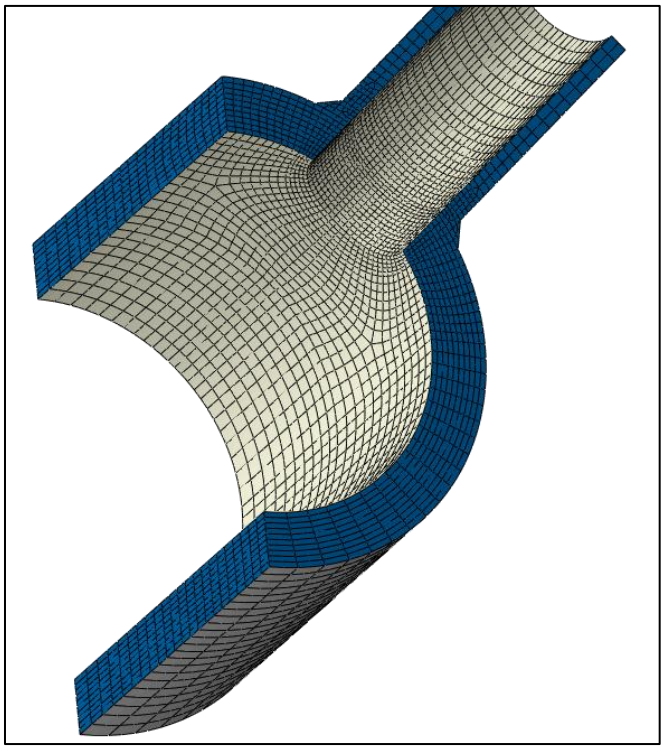

FIG. 4: UPDATED FINITE ELEMENT MODEL (1)

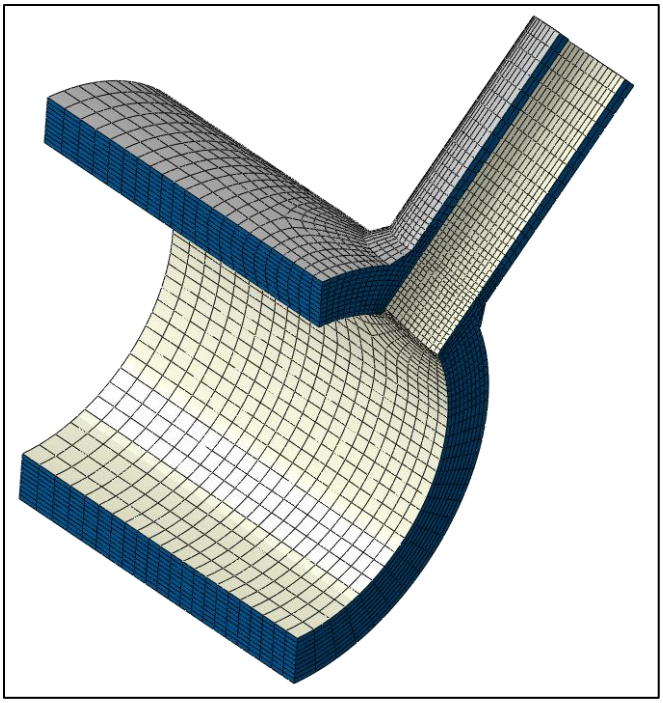

FIG. 5: UPDATED FINITE ELEMENT MODEL (2)

Equivalent stress results (von Mises type) for the updated model under design pressure loading are shown in Figure 6 (the results are shown with the model mirrored for illustration). These results show essentially the same results as Figure 2 (previous analysis) demonstrating elastic stress convergence; however, the finer mesh is retained here. The deformation is illustrated in Figure 7 for reference and verification purposes. These figures represent the results using quadratic elements, however results from the linear element analysis are essentially the same.

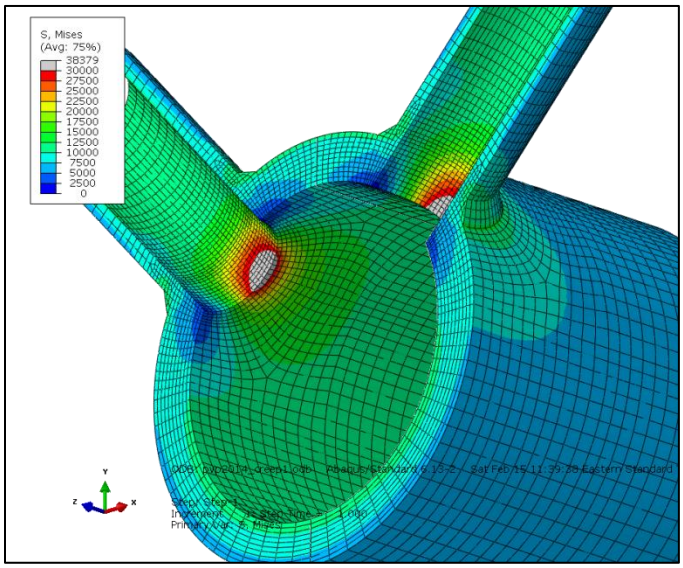

FIG. 6: CURRENT ELASTIC FEA DESIGN PRESSURE VON MISES STRESS RESULTS (in units of psi, 2575 psig, 17.754 MPa)

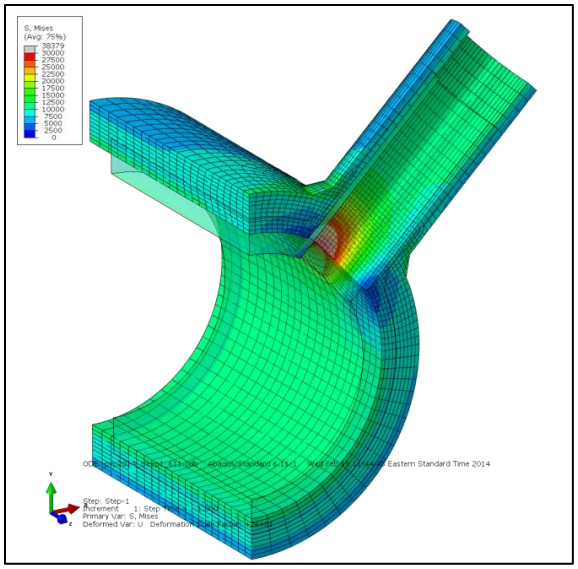

FIG. 7: CURRENT ELASTIC FEA DESIGN PRESSURE VON MISES STRESS RESULTS (psi) - DEFORMATION DETAIL (40x)

The method of assessing sub-creep regime elastic FEA results for Code compliance is stress classification (see for example Annex 5-A, "Linearization of Stress Results for Stress Classification" [12]). Recall from [10] that the inelastic analysis showed creep damage was maximum in the same location as the elastic stress concentration region of the stub penetration and propagated with time around the penetration and into the ligament. This (uniaxial) damage pattern then lines up with the elastic stress analysis contours, and the elastic analysis alone could be used to guide stress classification line selection. Consideration of multiaxial creep effects will likely complicate this conclusion, but that issue is saved for a subsequent discussion. The specific lines chosen are shown superimposed on the elastic equivalent (von Mises) stress results in Figure 8 and Figure 9.

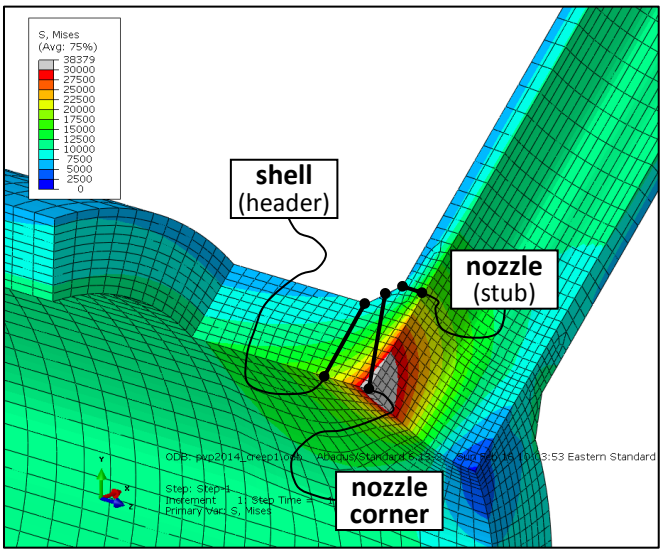

FIG. 8: STRESS LINEARIZATION LOCATIONS (1)

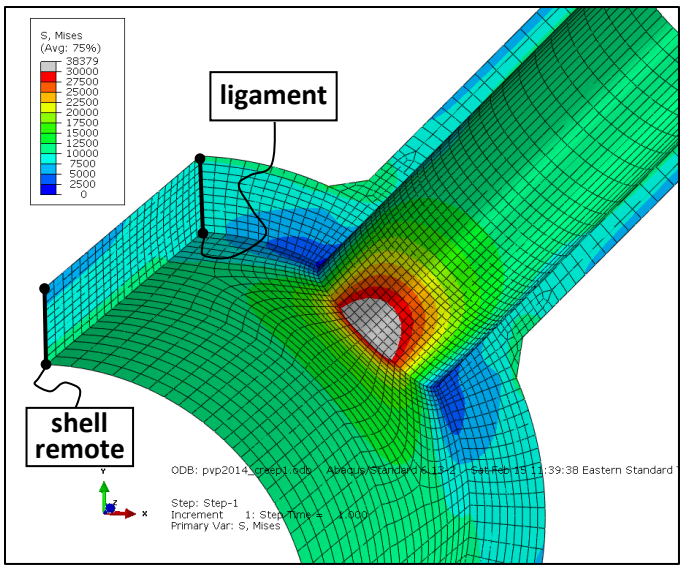

FIG. 9: STRESS LINEARIZATION LOCATIONS (2)

The lines shown in general correspond to the guidance in [12], [18] and [19]. Per [18], the nozzle corner location is not a valid failure plane (line), but would be allowed per [12] and [19]. Even in the case of [12] and [19] the nozzle corner location is not strictly valid because it does not meet the requirement that the line is oriented normal to the mid-surface of the cross section. This illustrates the primary difficulty of elastic analysis and stress linearization for three dimensional cases, though it remains a cornerstone of traditional DBA.

Note that in Figure 9 only one ligament line is shown, but several potential lines from the weld toe to the ligament center (ten lines in all corresponding to ten elements across the half-ligament) were checked and showed very similar results. The mid-ligament line is presented because it has the slightly higher membrane stress and similar bending stresses to the other locations.

Stress linearization results are presented in Table 2 (and Table 2M for metric units) and correspond to the Tresca equivalent stress for consistency with the intent of [2]. The von Mises results are similar however, and give identical trends to those shown. "P" is used to denote membrane (average) stresses, all of which are categorized as local with the exception of the "shell remote" location, which is general (see [12] for stress and classification definitions). "Q" is used to denote bending, which in all cases is a secondary bending here.

Table 2 also includes the results normalized by allowable. The allowables here are based on the rupture LMP that the creep curve is derived from for consistency, and not the exact Code allowable stress in this case. From [10], the consistent allowable stress is then:

100,000 hr. (average) rupture stress at 1085°F (585°C):

100%: 15.237 ksi (105.056 MPa)
67%: 10.209 ksi (70.388 MPa)

S(1085°F) = **10.21 ksi** (70.388 MPa)

And from [12],

General Primary Membrane Stress, $\mathbf{P_m < S}$ (10.21 ksi)
Local Primary Membrane Stress, $\mathbf{P_L < 1.5S}$ (15.31 ksi)
Membrane plus Bending Stress, $\mathbf{P + Q < 3S}$ (30.63 ksi)

The above membrane plus bending stress (less than P+Q case) is given for completeness, as there is debate over whether it has any meaning for non-cyclic operation. However, it can always be interpreted as a conservative deformation limit, and in this case is selected to help investigate the correspondence of potential limits relative to the detailed inelastic analysis results (see Figure 3 and [9]). Although [12] is primarily for non-creep operation, as long as fatigue screening checks are passed the above limits can in fact currently be applied even when the allowable stress is governed by creep properties.

As Table 2 shows the nozzle corner is the only location that violates the chosen limits. Recall that this location is not accepted as a generally valid classification location, although it does capture the highest stress location. If this line were excluded from consideration as invalid, then the elastic results would match the Design-by-Rule results (of [1] or [2]) which demonstrate the design is acceptable.

Further review of Table 2 shows an interesting result however; that is, the primary membrane (and membrane plus bending) stress in the ligament is essentially the same as in the remote shell. Since the header shell meets the allowable stress intent exactly (see [9]), this would suggest that the ligament region should actually meet the 100,000 hour requirement at 1.5x design load. Although as shown in Figure 3, this is not the detailed inelastic result, which predicts only a fraction of that time is reached before complete rupture of the ligament occurs. This means that the stress must actually be increasing in time as the load in the higher stressed penetration decreases. This is confirmed by the time history results for the stress and rupture fraction (damage) plotted in Figure 10. This is an important result, since not only does the (discontinuity region) stress not relax as expected (recall again [13]), it actually slightly increases with time!

TABLE 2
STRESS LINEARIZATION RESULTS FOR DESIGN PRESSURE

Location	**P** (ksi)	**Allowable Ratio**	**P + Q** (ksi)	**Allowable Ratio**
Nozzle Corner	20.55	1.34	34.93	1.14
Shell	15.00	0.98	19.19	0.63
Nozzle	14.16	0.92	18.59	0.61
Ligament	9.09	0.59	12.39	0.40
Shell Remote	9.96	0.89	11.23	0.37

TABLE 2M
STRESS LINEARIZATION RESULTS FOR DESIGN PRESSURE (METRIC UNITS)

Location	P (MPa)	Allowable Ratio	P + Q (MPa)	Allowable Ratio
Nozzle Corner	141.7	1.34	240.8	1.14
Shell	103.4	0.98	132.3	0.63
Nozzle	97.63	0.92	128.2	0.61
Ligament	62.67	0.59	85.43	0.40
Shell Remote	68.67	0.89	77.43	0.37

The elastic stress analysis is not capable of predicting a redistribution pattern such as this, which will lead shortly to investigation of isochronous curve analysis. Recall that this is not an indictment of experience-based rules, but rather part of a development for analysis-based rules that can complement experience.

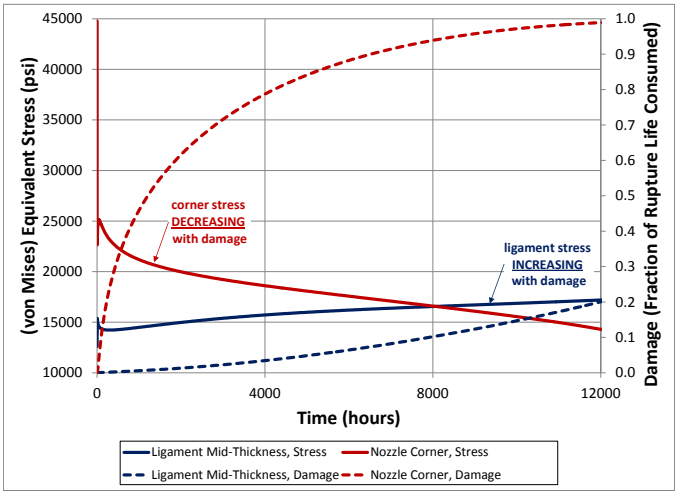

FIG. 10: STRESS REDISTRIBUTION HISTORIES FROM INELASTIC ANALYSIS

One of the reasons for presenting the elastic analysis in detail was to investigate the traditional (lower temperature, non-creep) DBA stress limits. Depending on the stress linearization locations, the example design can be shown to pass or fail. However, for the moment assuming that DBA might be desired as a means to introduce more consistent margin into a design, a natural question might be what elastic limits would avoid the result shown in Figure 3. For example, the following limits have been suggested:

General Primary Membrane Stress, $\mathbf{P_m < S}$ (10.21 ksi)
Local Primary Membrane Stress, $\mathbf{P_L < 1.25S}$ (12.25 ksi)
Membrane plus Bending Stress, $\mathbf{P + Q < 2S}$ (20.42 ksi)

The results of Table 2 are presented in Table 3 normalized simply by the above basic (assumed) allowable stress. As Table 3 shows, the (potentially invalid) nozzle corner location is no longer the only location that does not meet the stricter limits, as the shell and nozzle also have local membrane results greater than 1.25S. This is a positive result (relative to methods) since a single (controversial) location would no longer be controlling the analysis outcome. Recall that the standard way to avoid ambiguities relative to stress classification and failure planes in 3D is to perform limit load analysis. But as already mentioned and demonstrated in [10], such methods for the elevated temperature case may not be mature. This, along with its wider availability, makes elastic analysis relevant for investigation, even with the shortcoming relative to complex high temperature redistribution behavior already noted. However, another simplified method with promise of potentially capturing more relevant high temperature behavior (at the cost of increased complexity) will be evaluated next.

TABLE 3
STRESS LINEARIZATION RESULTS FOR DESIGN PRESSURE NORMALIZED BY BASIC ALLOWABLE STRESS

Location	(P)/S	(P + Q)/S
Nozzle Corner	2.01	3.42
Shell	1.47	1.88
Nozzle	1.39	1.82
Ligament	0.89	1.22
Shell Remote	0.89	1.21

ISOCHRONOUS CURVE ANALYSIS

Isochronous stress-strain curves have been used for elevated temperature design for many years (e.g. [3] and [4]). Their intent and use was described in the well-known document [20] that provides in part a basis for the curves in [3]. From [20] (L. D. Blackburn);

> "An isochronous curve simply presents, in a plot of stress against strain, the locus of total strains accumulated when different constant stresses are applied for a fixed time."

These curves contain both time independent (elastic and plastic) strains, as well as time-dependent creep strains. From [21], such curves can be easily generated from the Omega model with the following relationship:

$$\varepsilon(t) = -\frac{\ln\left(1-\Omega\dot{\varepsilon}_o t\right)}{\Omega} + \frac{\sigma}{E} + \varepsilon_{pl} \qquad (7)$$

For this example, comparison of the elastic stress magnitudes with the hot yield strength (see Table NH-I-14.5 of [3] for example, where S_y(1085°F) = 33.9 ksi or S_y(585°C) = 233.7 MPa) shows plastic strains are negligible, and the simpler elastic-creep form of the model can be used. Recall that the model constants in the above equation are the initial

strain rate $\dot{\varepsilon}_o(T,\sigma)$ and the Omega constant $\Omega(T,\sigma)$, which are given in Table 1 for the current case of Grade 91 material based on the rupture data of [22]. Here (T,σ) indicates that the parameters are functions of temperature and stress. Therefore, by fixing values of temperature and time, a continuous (isochronous) stress-strain curve can be generated by Equation (7). However, Equation (7) does not include primary creep, which was included in [9]. Primary creep is easily added though, following the discussion in [17] (and as demonstrated in [9]). With reference to Equation (6), the updated isochronous stress-strain curve is then:

$$\varepsilon(t) = \frac{\ln\left(1+\Omega_p \dot{\varepsilon}_{op} t\right)}{\Omega_p} - \frac{\ln\left(1-\Omega \dot{\varepsilon}_o t\right)}{\Omega} + \frac{\sigma}{E} \qquad (8)$$

At the header design temperature of 1085°F (585°C), the elastic modulus for Grade 91 is $24.68 \cdot 10^4$ ksi ($1.702 \cdot 10^6$ MPa). The resulting isochronous curves using average properties and 300,000 hours and minimum properties (LMP constant shift of 0.522, see [9]) with 100,000 hours are shown in Figure 11. Of note is that the curves corresponding to the chosen time-property combinations are nearly identical, and suggest a potentially reasonable relationship between design and operating life. As shown, this is true whether or not primary creep is included; however, the effect of the relatively strong primary creep assumed here is clear.

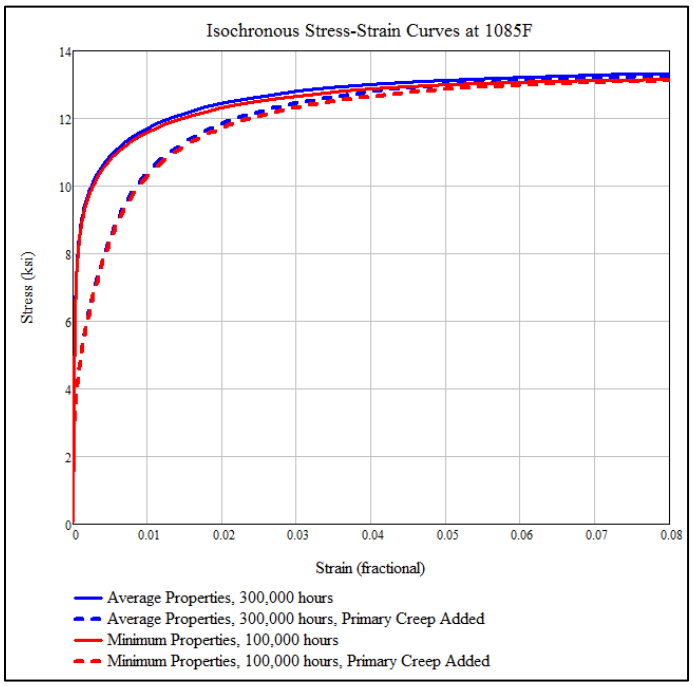

FIG. 11: ISOCHRONOUS STRESS-STRAIN CURVES GENERATED FOR GRADE 91 AT 1085°F

This type of curve can be input directly as (time-independent) stress-strain point pairs in common commercial FEA programs, which has the advantage of simplicity. Experience has shown that the stress and strains predicted from a time-independent analysis using an isochronous curve can give useful approximations of the actual time-dependent creep behavior. That is, the redistribution behavior and total strains predicted from a simple isotropic elastic-plastic analysis can in fact approximate the final state at the total time the isochronous curve is determined for.

The results of analyses using the curves of Figure 11 are shown in Figure 12 through 14 (average properties, with primary creep) and Figure 15 (minimum properties, with primary creep), both for design pressure. For use with the FEA code, only the inelastic strain is required, and a specific "yield" point needs to be defined. Therefore, the elastic strain (σ/E) is subtracted from Equation (8), and a conservative yield point of 2 ksi is assumed in both cases (average and minimum properties). The inelastic strain at the yield point is taken as zero, and all other strain (and stress) values are left unchanged.

As inferred above, these types of analyses typically use the actual design pressure as opposed to a factored load, and limits are placed on the resulting strain. In this case, the limits of III-NH [3] are chosen for evaluation, which are as follows:

Membrane strain limit:	1%
Membrane plus bending strain limit:	2%
Total strain limit:	5%

Where the total strain limit is assumed to apply at any point. For comparison to these limits, Figures 12 through 15 show contours of equivalent (pseudo-plastic) strain, denoted as "PEEQ". This is an accumulated quantity in Abaqus, but since no reverse loading and yielding is taking place, is exactly equal to the (instantaneous) equivalent plastic strain magnitude in this case. The term pseudo-plastic is used since the isochronous curve is really representing an equivalent creep strain after a given time.

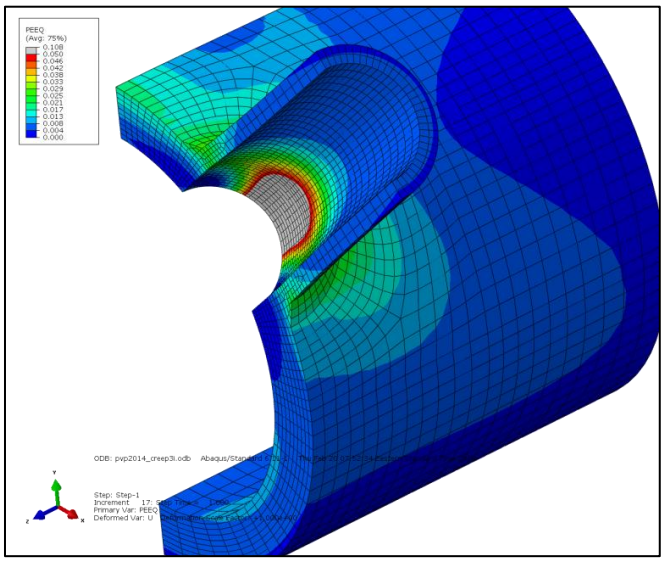

FIG. 12: ISOCHRONOUS CURVE ANALYSIS RESULTS, 300,000 HOUR AVERAGE PROPERTIES - 5% STRAIN CONTOUR CAP

As shown in Figure 12, the maximum strain is 10%, and large quantities of material are in excess of 5% strain. This is illustrated through-thickness in the detail of Figure 13. Clearly the 2% strain limit would not be met either based on this contour result, and detailed strain linearization is not pursued. Figure 14 shows the same results but with the contour scale capped at 1%, and the similarity to the detailed creep analysis results already presented (Figure 3) is striking. Only a single plot of the 100,000 hour minimum property case is given in Figure 15, to show that the results are essentially identical to the average property 300,000 hour case. This is as expected, since the input curves are essentially identical as shown in Figure 11.

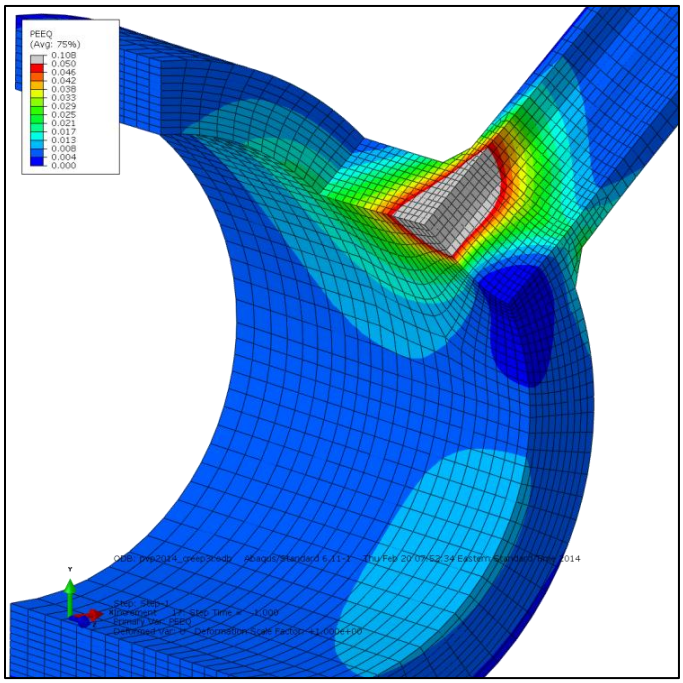

FIG. 13: ISOCHRONOUS CURVE ANALYSIS RESULTS, 300,000 HOUR AVERAGE PROPERTIES - 5% STRAIN CONTOUR CAP - DETAIL

It is possible that the example primary strain contribution included here (and in [9] and [10]) is over-influencing these strain results. Clearly the isochronous curves illustrated in Figure 11 suggest that several percent of equivalent strain are in fact due to the primary creep strain. While primary creep strain is likely important for Grade 91, the specific magnitudes predicted here are extremely approximate since primary creep strain data in parametric form is scarce in general. However, for consistency with the preceding analysis ([9] and [10]), the primary creep addition is retained, and analysis excluding primary creep effects is not presented for brevity.

Based on the isochronous curve analysis alone, one would have to conclude that the strain limits are not met and that the design is unacceptable. As mentioned, without primary creep, the design would be much closer to acceptable. Also recall that the primary creep question did not influence the results of the previous analyses in [10] since the fraction of rupture life consumed is independent of it in the Omega model (see [9] for more discussion), but this does illustrate the potential difficulty in both design property availability and specific strain limit choice.

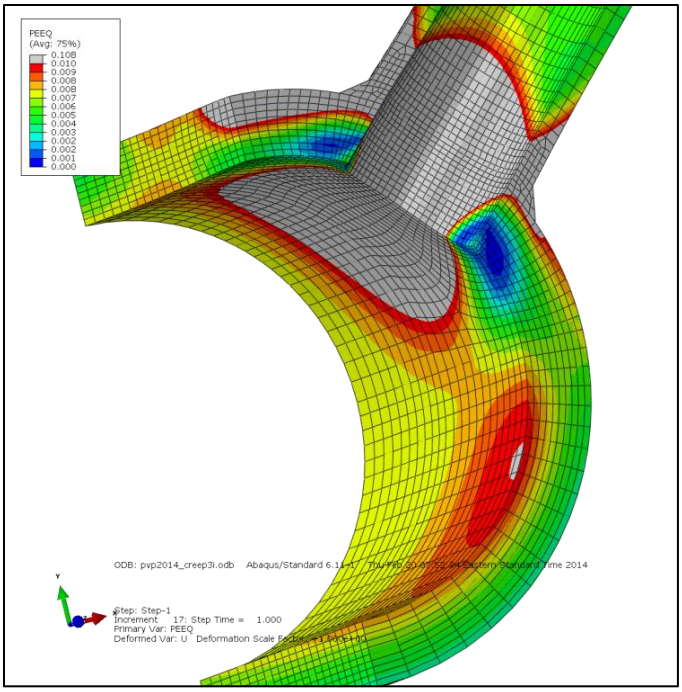

FIG. 14: ISOCHRONOUS CURVE ANALYSIS RESULTS, 300,000 HOUR AVERAGE PROPERTIES - 1% STRAIN CONTOUR CAP

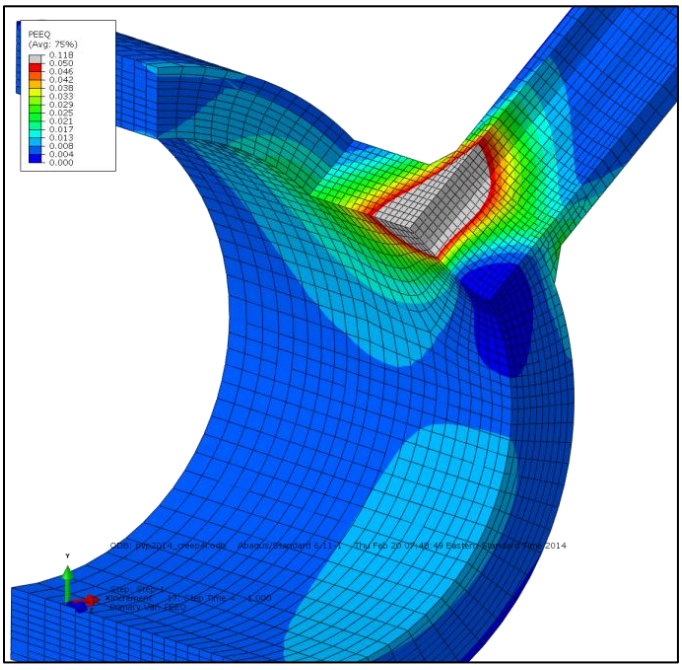

FIG. 15: ISOCHRONOUS CURVE ANALYSIS RESULTS, 100,000 HOUR MINIMUM PROPERTIES - 5% STRAIN CONTOUR CAP

For comparison purposes, the predicted strains after 300,000 hours of detailed creep analysis using average creep properties with the design pressure are shown in Figure 16, which can be directly compared with the corresponding isochronous curve results in Figure 13. Figure 17 shows the results of detailed analysis after 100,000 hours using minimum creep properties and can be directly compared with the corresponding isochronous curve results in Figure 15. Both the isochronous curve and creep analyses consider nonlinear geometric effects.

Comparison of the simplified isochronous curve analysis with the detailed creep analysis results shows that the isochronous analysis does an excellent job of predicting both strain magnitudes and distributions. The larger result of this is that isochronous analysis has the ability to overcome (by its fidelity to the more detailed and complex time-dependent creep analysis) some of the difficulties noted with elevated temperature elastic analysis. However, a remaining complication yet to be addressed is multiaxial creep effects. This topic is introduced in the next section.

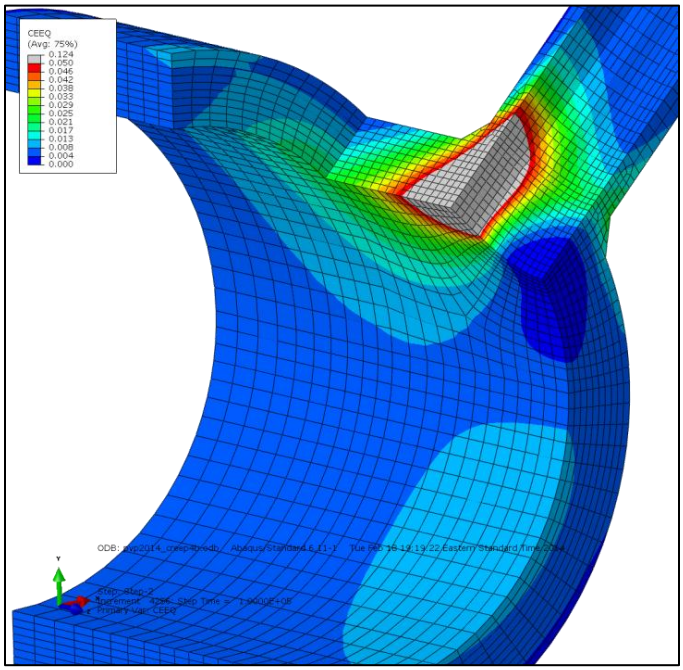

FIG. 16: DETAILED CREEP ANALYSIS RESULTS, 300,000 HOURS, AVERAGE PROPERTIES - 5% STRAIN CONTOUR CAP

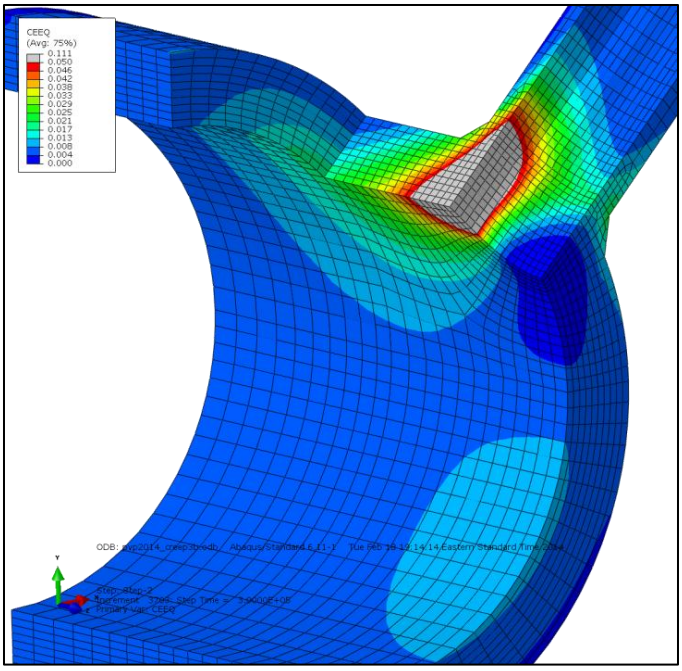

FIG. 17: DETAILED CREEP ANALYSIS RESULTS, 100,000 HOURS, MINIMUM PROPERTIES - 5% STRAIN CONTOUR CAP

TRIAXIAL STRESS STATE EFFECTS

Consideration has been restricted to uniaxial creep properties to this point so that the relevant complexities could be systematically built to. The next major topic (or complexity) to be investigated is extension of material modeling to the more general multiaxial case. Basic multiaxiality is treated by use of an equivalent stress (such as Tresca or von Mises) and is applied in all cases (even the "uniaxial" analysis presented in this paper). However, creep multiaxiality has a specific connotation and refers to the change in strain rate, ductility and rupture behavior with different multiaxial stress states.

Substantial debate and a corresponding variety of multiaxial corrections exist to address these observed effects, although the numerical range of differences may be less than might be expected. Regardless of model, multiaxial effects can be pronounced though; for example, analysis using the multiaxial Omega model from [6] are shown in Figure 18.

The striking aspect of this example (but typical) result is that the location of maximum damage has shifted to the reinforcement weld region, and predicted damage in the header itself is much more widespread. These results can be understood in part simply by looking at the elastic principal stresses, and the corresponding von Mises and pressure (hydrostatic) stresses, which are shown in Table 4 (and Table 4M).

In Table 4 σ_1 is the first principal stress, etc., σ_e is the von Mises equivalent stress and σ_h is the pressure or hydrostatic stress. Note that these linearized stresses are slightly different than those underlying Table 2 because all stress components are included in the linearization. Table 2 reflects Annex 5-A [12] guidance where the -11, -12 and -13 local direction

bending is not included in the principal or equivalent stresses. The ratio shown in Table 4 is the typical indicator of triaxiality. While the P and P+Q equivalent stresses are almost the same for the two (shell) regions in Table 2, clearly the underlying stress state is quite different.

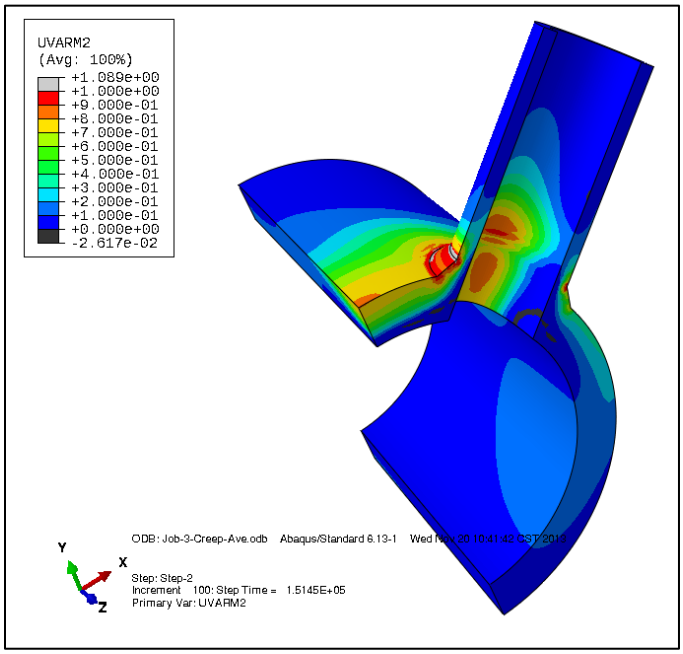

FIG. 18: EXAMPLE OF INCLUSION OF MULTIAXIAL CREEP EFFECTS INTO TIME-DEPENDENT INELASTIC ANALYSIS

TABLE 4
SHELL AND LIGAMENT LINEARIZED (P+Q) ELASTIC STRESS STATES

Location	σ_1 (ksi)	σ_2 (ksi)	σ_3 (ksi)	σ_e (ksi)	$3\sigma_h/\sigma_e$
Ligament	11.12	9.25	0.51	10.26	2.0
Shell (remote)	10.09	3.67	-2.42	10.84	1.0

TABLE 4M
SHELL AND LIGAMENT LINEARIZED (P+Q) ELASTIC STRESS STATES (METRIC UNITS)

Location	σ_1 (MPa)	σ_2 (MPa)	σ_3 (MPa)	σ_e (MPa)	$3\sigma_h/\sigma_e$
Ligament	76.67	63.78	3.52	70.74	2.0
Shell (remote)	69.57	25.30	-16.69	74.74	1.0

Changes in creep behavior even for a simple cylinder under internal pressure is a real effect. For example, see Page 173-174 of [23], where in discussing steady state creep under multiaxial stress it is noted that in a typical boiler or furnace tube,

> " . . . the tangential strain rate [from strain rate measurements] is less than one-third the strain rate that would be produced by the tangential stress acting alone in a tension test."

From a strain perspective this would appear to be good news; however, the reduced strain rate is accompanied by an accelerated damage, and the topic is not so simple after all. Furthermore, [23] states:

> "Furnace tube retirement is often based on maximum increase of outside diameter which experience shows will correspond to a certain future life. Unless the preceding type of calculation is used, a comparison with tensile creep data has little meaning."

Which is a caution that strain limits may also need to be based on the stress state rather than a set of unique values as in [3]. Examples of such an approach are provided by the time independent local strain criteria in [12] or the multiaxial damage criteria in [6].

In terms of the design approaches presented here, rigorous incorporation of such creep multiaxiality effects would seem to be a significant challenge. However, options do exist. For example, use of plasticity theories with a pressure stress dependence might allow multiaxial effects to be accommodated with a relatively simple isochronous curve analysis. On the other hand, simply using modified rupture values that reflect common multiaxial situations might be useful, or alternate elastic analysis limits and triaxial stress checks might bound these effects.

SUMMARY AND CONCLUSIONS

Elastic analysis with stress linearization and isochronous stress-strain analysis with strain limits have both been evaluated. In each case, the detailed inelastic creep analysis presented in [9] and [10] and extended here is used as the reference solution. A primary finding of this work is that the ligament stress is predicted to actually increase with time and creep damage in the elevated temperature case, which is directionally consistent with the results of [13]. This suggests that elastic analysis may prove to be difficult to use reliably for elevated temperature DBA, although the possibility of using stricter limits was illustrated (1.25S and 2S versus 1.5S and 3S) and shows some promise. This may in fact be feasible since analysis is being restricted to pressure vessel components and details, and not truly arbitrary configurations. Such an approach (in fact any approach) would need to therefore be validated against a wide range of sample configurations before general use.

Inelastic analysis with consistent isochronous curves was shown to overcome this difficulty, and in fact g strain results nearly identical to detailed time-dependent creep analysis. While inelastic analysis is undoubtedly more challenging than

elastic analysis for the general FEA practitioner, the improvement in predictive ability is very significant.

The effects of multiaxiality on these results was also introduced. In terms of design modernization, once creep multiaxiality effects are defined and bounded to the extent possible, the remaining task is to incorporate this effect consistently into design evaluations. This is the current focus of further work, in support of the on-going design modernizations taking place within Section 1 and Section VIII Division 2 of the ASME Code.

NOMENCLATURE

$a_0 \ldots a_4$	=	Omega model initial strain rate function coefficients
$b_0 \ldots b_4$	=	Omega model Omega parameter function
E	=	elastic modulus
P	=	primary membrane stress intensity
P_m	=	general primary membrane stress intensity
P_L	=	local primary membrane stress intensity
Q	=	secondary bending stress intensity
S	=	allowable stress
S_l	=	base 10 logarithm of true stress
t	=	time
T	=	temperature
T_{abs}	=	absolute temperature (K or R)
ε	=	total (elastic, plastic, creep) strain
ε_{pl}	=	plastic strain
$\dot{\varepsilon}_c$	=	true creep strain rate
$\dot{\varepsilon}_o$	=	initial tertiary true creep strain rate
$\dot{\varepsilon}_{op}$	=	initial primary true creep strain rate
$\dot{\varepsilon}_p$	=	primary true creep strain rate
$\dot{\varepsilon}_t$	=	tertiary true creep strain rate
σ_1	=	first principal stress, etc.
σ_e	=	von Mises equivalent stress
σ_h	=	hydrostatic or pressure stress
Ω	=	Omega model tertiary parameter
Ω_p	=	Omega model primary parameter

REFERENCES

1. ASME Boiler and Pressure Vessel Code, 2013, Section I, "Power Boilers," American Society of Mechanical Engineers, New York.
2. ASME, 2013, ASME Boiler & Pressure Vessel Code, Section VIII, Division 1, American Society of Mechanical Engineers, New York.
3. ASME Boiler and Pressure Vessel Code, 2013, Section III, Subsection NH, American Society of Mechanical Engineers, New York.
4. R5: Assessment procedure for the high temperature response of structures, Volume 2/3, "Creep-Fatigue Crack Initiation Procedure for Defect-Free Structures," Revision 3. June 2003.
5. API Recommend Practice 579 (API RP 579), Fitness-For-Service, 1st Edition, The American Petroleum Institute, 2000.
6. API 579-1/ASME FFS-1, Fitness-For-Service, 2nd Edition, The American Petroleum Institute, 2007.
7. Prager, M. "Development of the MPC Omega Method for Life Assessment in the Creep Range," ASME PVP Volume 288, The American Society of Mechanical Engineers, New York, N.Y., 1994.
8. Prager, M., "The Omega Method – An Effective Method for Life and Damage Prediction in Creep Tests and Service," International Conference of the Strength of Materials, The Japan Institute of Metals, 1994.
9. Dewees, D. J. and R. Jain, "Evaluation of Limit Load Analysis Methods Applied to High Temperature Design, Part 1: Consistent Material Modeling," ETS2014-1039, ASME Symposium on Elevated Temperature Application of Materials for Fossil, Nuclear and Petrochemical Industries, ASME, New York, March 25-27, 2014.
10. Dewees, D. J. and R. Jain, "Evaluation of Limit Load Analysis Methods Applied to High Temperature Design, Part 2: Analysis and Results," ETS2014-1042, ASME Symposium on Elevated Temperature Application of Materials for Fossil, Nuclear and Petrochemical Industries, ASME, New York, March 25-27, 2014.
11. Cao, Z., L. Bildy, D. A. Osage and J. Sowinski, 2010, "Development of Nozzle Rules for ASME B&PV Code Section VIII Division 2," WRC Bulletin 529, The Welding Research Council, Inc., New York.
12. ASME Boiler and Pressure Vessel Code, 2007, Section VIII, "Rules for Construction of Pressure Vessels," Division 2, "Alternative Rules," American Society of Mechanical Engineers.
13. Becht IV, C., "Behavior of Pressure-Induced Discontinuity Stresses at Elevated Temperature," Journal of Pressure Vessel Technology, Vol. 111, August 1989. American Society of Mechanical Engineers, New York.
14. Albrecht, M. J., et. al., "Use of a Vertical Separator Design for a Natural Circulation HRSG Boiler," PowerGen 2012.
15. DSS SIMULIA Corp., Abaqus Finite Element Software, version 6.11-1 through 6.13-2, 2010-2013.
16. ASME Boiler and Pressure Vessel Code, 2007, Section II, "Materials," Part D, "Properties," American Society of Mechanical Engineers, New York.
17. Prager, M., "Background Materials Issues in CC2605 for 2¼Cr-1Mo-V – Potential to Extend to Other Creep Strength Enhanced Ferritic (CSEF) Steel Materials: Application of a Concept of Damage," Presented to the

ASME Subgroup on Elevated Temperature Construction (Sc-III), Phoenix, AZ. November 2012.
18. Hechmer, J. L. and G. L. Hollinger, 1998, "3D Stress Criteria Guidelines for Application," WRC Bulletin 429, The Welding Research Council, Inc., New York.
19. Kroenke, W.C. "Classification of Finite Element Stresses According to ASME Section III Stress Categories," Proceedings of the 1974 Pressure Vessels and Piping Conference, Miami Beach, FL, Pressure Vessels and Piping: Analysis and Computers. ASME, 1974.
20. "The Generation of Isochronous Stress-Strain Curves," Presented at the Winter Annual Meeting of the ASME, November 26-30, 1972. A. O. Schaefer, Ed., American Society of Mechanical Engineers, New York.
21. Prager, M., "Generation of Isochronous Creep, Tubing Life and Crack Growth Curves Using the MPC Omega Method," Structural Integrity, NDE, Risk and Material Performance for Petroleum, Process and Power, PVP-Vol. 336, ASME, 1996, pp. 303-322.
22. Prager, M., D. A. Osage and C. H. Panzarella, "Evaluation of Material Strength Data for Use in API Std 530," WRC Bulletin 541, The Welding Research Council, Inc., New York, N.Y., 2012.
23. Creep of Engineering Materials, Iain Finnie and William H. Heller, McGraw-Hill Book Company, New York. 1959.

ANNEX A

ISOCHRONOUS STRESS-STRAIN CURVE CALCULATIONS

The isochronous curves used for analysis presented in this paper are developed using the Omega model and data as presented in Table 1 and [9]. Specifically, using the software Mathcad;

Initial strain rate:

$$\varepsilon'_o(T,\sigma,a) := 10^{-\left(a_0+\frac{a_1+a_2\cdot\log(\sigma)+a_3\cdot\log(\sigma)^2+a_4\cdot\log(\sigma)^3}{T}\right)}$$

Initial strain rate coefficients, average properties (units = ksi, R):

$$A_{530.ksi.\Omega} = \begin{pmatrix} -32.36 \\ 70650.00 \\ -2880.00 \\ -5139.53 \\ 0.00 \end{pmatrix}$$

Initial strain rate coefficients, minimum properties (units = ksi, R):

$$A'_{530.ksi.\Omega} := \begin{pmatrix} -32.36 - 0.522 \\ 70650.00 \\ -2880.00 \\ -5139.53 \\ 0.00 \end{pmatrix}$$

Omega parametric expression:

$$\Omega(T,\sigma,b) := 10^{b_0+\frac{b_1+b_2\cdot\log(\sigma)+b_3\cdot\log(\sigma)^2+b_4\cdot\log(\sigma)^3}{T}}$$

Omega coefficients (average or minimum properties, ksi, R):

$$B_{530.ksi.\Omega} = \begin{pmatrix} -2.00 \\ 7200.00 \\ -1500.00 \\ 0.00 \\ 0.00 \end{pmatrix}$$

Temperature for evaluation:

$$1085\,°F = 1544.67\cdot R$$

Assumed primary creep strain ratios:

$$R_\Omega := 20 \qquad R_\varepsilon := 200$$

For the isochronous curve, fix temperature, specify coefficients:
(average property case shown)

$$\varepsilon'_{o.i}(\sigma) := \varepsilon'_{o}\left(1544.67, \sigma, A_{530.ksi.\Omega}\right)$$

$$\Omega_i(\sigma) := \Omega\left(1544.67, \sigma, B_{530.ksi.\Omega}\right)$$

Isochronous curve equation considering primary creep:

$$\varepsilon'(t,\sigma) := \frac{\ln\left(1 + R_\Omega \cdot \Omega_i(\sigma) \cdot R_\varepsilon \cdot \varepsilon'_{o.i}(\sigma) \cdot t\right)}{R_\Omega \cdot \Omega_i(\sigma)} - \frac{\ln\left(1 - \Omega_i(\sigma) \cdot \varepsilon'_{o.i}(\sigma) \cdot t\right)}{\Omega_i(\sigma)} + \frac{\sigma}{E}$$

where a specific σ-ε curve is generated by fixing the time, t (in hours)

The specific tabular data used in the FEA is shown in Table A.1. Note that this data does not include the elastic strain contribution, as required by the FEA.

TABLE A.1
ISOCHRONOUS CURVE TABULAR DATA USED IN ANALYSIS

Stress (psi)	**Inelastic Strain** Average Properties, 300,000 Hours	**Inelastic Strain** Minimum Properties, 100,000 Hours
2000	1.7838E-05	1.9512E-05
3000	9.6905E-05	1.0501E-04
4000	3.5005E-04	3.7287E-04
5000	8.6280E-04	9.0345E-04
5500	1.2158E-03	1.2649E-03
6000	1.6278E-03	1.6853E-03
6500	2.0972E-03	2.1636E-03
7000	2.6264E-03	2.7032E-03
7500	3.2230E-03	3.3130E-03
8000	3.9013E-03	4.0091E-03
8500	4.6852E-03	4.8181E-03
9000	5.6122E-03	5.7820E-03
9500	6.7400E-03	6.9654E-03
10000	8.1582E-03	8.4690E-03
10500	1.0008E-02	1.0453E-02
11000	1.2519E-02	1.3183E-02
11500	1.6093E-02	1.7137E-02
12000	2.1506E-02	2.3279E-02
12500	3.0577E-02	3.4073E-02
13000	4.9703E-02	6.0580E-02
13100	5.6917E-02	7.3437E-02
13200	6.7249E-02	1.0040E-01
13300	8.4969E-02	--
13400	1.6348E-01	--